Contents lists available at ScienceDirect

Arabian Journal of Chemistry

journal homepage: www.ksu.edu.sa

Original article

Fluorescent sensing of rutin by carbon dots derived from the heart of cumin seeds

Xiao-Lin Xie [a,1], Zhao Zhang [b,1], Wen Xiong [b], Jie Wang [a], Wei Gong [a], Wen Xu [a], Shuang Cai [b], Jing Li [a,*]

[a] Xiangyang Central Hospital, Affiliated Hospital of Hubei University of Arts and Science, Xiangyang 441021, China
[b] Department of Chemical Engineering and Food Science, Hubei University of Arts and Science, Xiangyang 441053, China

ARTICLE INFO

Keywords:
Carbon dots
Cumin embryo
Rutin
Biomass
Fluorescent sensor

ABSTRACT

Carbon dots (CDs) prepared from biomass usually produce poor quantum yield and reproducibility. A fine separation of raw materials may enhance the fluorescence performance. In this work, embryos of cumin seeds were precisely chosen as the carbon source to prepare (CDs) through hydrothermal method. The obtained product (CDs-E) possessed a higher quantum yield of 10.60 % than those synthesized with testas or whole seeds, which may be due to the relatively smaller particle size and more C-N functional groups. Rutin, as a common natural active component, could quench the fluorescence of CDs-E notably through internal filtering effect. Herein, a highly selective fluorescent sensor based on CDs-E for detecting rutin was proposed with a linearity range of 0.05 ~ 30 μM and a detection limit of 0.015 μM obtained. Additionally, the developed method was successfully applied for the detection of rutin in *Flos Sophorae*, rutin tablets and capsules. This work showed the significance of fine classification for natural carbon source in preparation of CDs and provided a feasible method for quality monitoring of rutin-related pharmaceuticals, health care products and traditional Chinese medicinal materials.

1. Introduction

Rutin has a variety of biological activities, including but not limited to anti-inflammatory, anti-adipogenic, anti-oxidation, anti-aging effects, thus being extensively used in the treatment of related diseases and possesses affirmative curative effect (Chua, 2013). Drugs and health care products containing rutin, such as tablets and capsules, is common and easy to obtain. Chinese Pharmacopoeia has also included many kinds of traditional Chinese medicinal (TCM) materials and decoction pieces with rutin as the index for quality control. Nevertheless, excessive consumption of rutin can cause side effects and even toxicity, for instance headache, tachycardia, nervousness, rash and blurred vision (Hasumura et al., 2004). Hence, quantity monitoring of the drugs, health care products and TCM was essential to ensure the efficiency and safety of rutin intake. Conventional approaches for rutin detection span high-performance liquid chromatography (HPLC), capillary zone electrophoresis and electrochemical methods, which require relatively high equipment configuration and technical personnel (Wang et al., 2023). Thereby, ultrasensitive and cost-effective methods are still worth exploring.

In recent decades, carbon dots (CDs) have attracted considerable attention as fluorescent nanomaterials due to their low toxicity, good biocompatibility, simplicity in preparation, and excellent fluorescence properties. After years of effort, researchers have successfully applied them to biosensors, batteries, catalysis, imaging, and other fields (Ji et al., 2020, Wang et al., 2021). Involuntary, it is a right direction for extending the application of CDs to detect rutin. Researchers have designed CDs-based sensing systems for rutin, and the CDs were all almost chemically derived (Sinduja and John, 2018, Li et al., 2019, Wang et al., 2019, Huang et al., 2022, Mahmoud et al., 2022, Xie et al., 2022, Zhang et al., 2022, Wang et al., 2023). It is proverbial that the properties of CDs are greatly influenced by the carbon source used in the synthetic procedure. Specifically, the element composition and structural characteristics of CDs are highly dependent on the carbon precursors (He et al., 2022). The surface functional groups on CDs which largely determine the chemical and photoluminescence properties are

* Corresponding author.
E-mail address: Lijing@hbuas.edu.cn (J. Li).
[1] Xiao-Lin Xie and Zhao Zhang contributed to this work equally.

https://doi.org/10.1016/j.arabjc.2024.105888
Received 14 April 2024; Accepted 25 June 2024
Available online 26 June 2024

also mainly inherited from the original carbon source (Ai et al., 2021). Thus, selection and exploration of appropriate carbon source are crucial for the development of novel CDs with tailored properties for specific applications.

Biomass, consisting of various components with diverse chemical properties, is a great candidate for producing CDs with specific properties (Liu et al., 2021, Wareing et al., 2021). However, CDs prepared from natural sources are usually low in quantum yield and their fluorescence properties cannot be perfectly replicated between batches due to high variations (Meng et al., 2019). In order to address these problems and expand the application scope of CDs, it remains an exciting and also interesting area to explore new biomass as carbon source of CDs. Cumin seed, a popular cooking spice which contains high carbohydrate, fat, protein, mineral, and vitamin content, is an excellent candidate for CDs production (Merah et al., 2020). Biomass was generally used as a whole in the production of CDs, cumin is no exception (Kaur et al., 2021). In general, different parts of biomass have varying chemical compositions, but the chemical composition of the same part is relatively stable. Likewise, cumin seeds can be divided to testas outside and embryos inside, which have quite different components (Merah et al., 2020). Therefore, it is possible to adjust the properties of CDs more accurately and ensure repeatability by choosing specific parts instead of bulk biomass as the carbon precursor. To our knowledge, it is the first work to compare the distinctions of CDs prepared with the subdivided parts of biomass in detail.

In this work, separate batches of CDs were prepared with cumin embryos, testas and the whole seeds respectively through the hydrothermal method and compared in detail. CDs derived from embryos (CDs-E) has higher quantum yield, smaller size and more C-N groups. Under the optimal conditions, CDs-E can be quenched by rutin selectively, thus a fluorescent sensor for rutin was established and successfully utilized in various samples, including drugs, health care products and TCM.

2. Experimental

2.1. Materials and reagents

Cumin seeds were bought from a local market. *Flos Sophorae* from different producing areas (PA), rutin tablets and capsules were obtained from a local hospital and three pharmacies. Methanol, HAcO, HCl, NaOH, NaCl, KCl, KI, KNO_3, $Al(NO_3)_3$, $CuSO_4$, $FeCl_2$, $FeCl_3$, $ZnCl_2$, $MgSO_4$, $AgNO_3$, $K_2Cr_2O_7$, $MnCl_2$, and $NaHCO_3$ of analytical grade were purchased from Sinopharm Chemical Reagent Co., Ltd. (Shanghai, China). Digitoxin (Dig), arbutin (Arb), naringin (Nar), quercetin (Que), isorhamnetin (Irh), kaempferin (Kae), ascorbic acid (VC), proline (Pro), glycine (Gly), histidine (His) and glutamic acid (Glu) were delivered by Aladdin Chemical Reagent Co., Ltd. (Shanghai, China). Ultrapure water was prepared by an LUE-20 water purification system (HyperPureX, China).

2.2. Apparatus

Fluorescence spectra and Ultraviolet–Visible absorption spectra were recorded on an F-4700 fluorescence spectrophotometer (Hitachi, Japan) and a P2 UV–vis spectrophotometer (Mapada, China), respectively. An ME 155DU analytical balance and a FiveEasy Plus pH meter (Mettler-Toledo, Switzerland) were employed for weighing and pH adjustment. A DGG-7090B air blast drying oven (Senxin, China) was utilized to provide high temperature environment. The morphology and dimension of the CDs were observed by a Dimension Edge Atomic Force Microscope (Bruker, USA) and a JEM-2100 microscope (JEOL, Japan) and the size statistics was conducted by a Nano Measure 1.2 software. The chemical composition and functional groups of the CDs were analyzed through Fourier transform infrared spectra (FTIR) and X-ray photoelectron spectroscopy (XPS) spectra, which were conducted on an AVATAR 360 FT-IR spectrometer and an ESCALAB 250Xi electron spectrometer (Thermo-Fisher, USA), respectively. The crystal pattern of the CDs was characterized through a 6100 X-ray diffractometer (Shimadzu, Japan). Detection of rutin through HPLC method was accomplished on an Ultimate 3000 HPLC system (Thermo-Fisher, USA) including pump, autosampler, column oven and diode array detector.

2.3. Synthesis and the properties inspection of CDs

For raw materials preparation, the cumin seeds were washed with ultrapure water, followed by dried and grinded. To separate testas and embryos, the whole seeds were rubbed mechanically in a mortar and then immersed in warm water for 4 h. Due to different densities, the testas floated and the embryos sank, thus separation was achieved naturally. They were collected and dried at 80 °C severally, and then crushed into powder with a grinder for backup.

For a typical procedure of CDs preparation, 2.0 g of the aforementioned powder was dispersed in 10.0 mL of ultrapure water with vortex to create a homogenous solution firstly. The resulting solution was then transferred into a Teflon-lined stainless-steel autoclave and subsequently heated to 200 °C, maintaining this temperature for a duration of 12 h. After naturally cooling down to room temperature, the products were collected and filtered through a 0.22 μm nylon filter, followed by dialysis against ultrapure water for 48 h within a dialysis tube (MWCO1000). Finally, the dialysate was vacuum evaporated and dried to yield the solid for further use.

For optimization of the preparation conditions of CDs-E, the input amount of cumin embryos (0.5 g ~ 3.0 g), hydrothermal temperature (140 °C ~240 °C) and hydrothermal time duration (6 h ~ 30 h) were investigated respectively. The quantum yield (QY) of the CDs was adopted as the indicator for optimization and measured with quinine sulfate as a reference (QY: 54 % at E_x of 360 nm in 0.1 M H_2SO_4). The QY of the as-prepared CDs was calculated according to Eq (1):

$$QY_S = \left(QY_R \cdot K_S \cdot \eta_S^2\right) / \left(K_R \cdot \eta_R^2\right) \quad (1)$$

where K is the slope of the linear fitted curve of fluorescence integrated area versus absorbance of CDs at different concentration; η is the refractive index of the solvent (1.33 for both pure water and 0.1 M H_2SO_4); The subscript R and S stand for the reference and sample, respectively.

The UV–Vis spectrum, excitation and emission spectra of CDs-E preparing under the optimum conditions were recorded to reveal the essential optical properties. The emission spectra at different excitation wavelengths (300 ~ 420 nm) were also recorded. To investigate the fluorescence stability of CDs-E, the pH was adjusted to 1 ~ 12 with HCl or NaOH solution and the ionic strength was controlled by different addition amount of NaCl (0 ~ 1.0 M), and the CDs-E solutions was continuously irradiated with ultraviolet of 355 nm for 120 min in the case of photostability.

2.4. Fluorescent sensing of rutin

Rutin was dissolved in methanol and configured to a concentration of 300 μM as a stock solution and diluted to standard working solution series with ultrapure water (0.05 ~ 30 μM). For a typical sensing process, 0.5 mL of the three CDs solution (100 μg mL^{-1}, in ultrapure water) was added to 4.0 mL of rutin solution. The mixture was incubated for 3 min in a shaker at 25 °C. The fluorescence intensity (F) of the solution was then measured at E_x of 355 nm and E_m of 430 nm. F_0 is the fluorescence intensity when the rutin solution was replaced by ultrapure water. The quenching efficiency (F/F_0) was calculated and the linear correlation analysis with the concentration of rutin was performed; The limit of detection (LOD) was calculated at the signal to noise ratio of 3.

For optimization of sensing conditions, the pH value of rutin solution was adjusted to 3 ~ 10 with HCl or NaOH solutions. The incubation time

and temperature ranged from 0.25 ~ 30 min and 4 ~ 65 °C, respectively. For evaluation of selectivity, rutin solution was replaced by K^+, Na^+, Mg^{2+}, Al^{3+}, Zn^{2+}, Cu^{2+}, Fe^{2+}, Fe^{3+}, Ag^+, Mn^{2+}, Cr(VI), I^-, Cl^-, NO_3^-, SO_4^{2-}, HCO_3^-, Dig, Arb, Nar, Que, Irh, Kae, VC, Pro, Gly, His and Glu solution at a concentration of 25 μM, respectively; For investigation of anti-coexisting interference, each substance aforementioned at a concentration of 10 μM was introduced into rutin working solution (2.5 μM). Then the sensing procedure was executed and the corresponding fluorescence intensity was compared with the case of rutin alone.

2.5. Application of real samples

For sample pretreatment, twenty rutin tablets were weighed and the average tablet weight was calculated. Then, they were powdered and mixed in a mortar. Portions equivalent to one tablet were weighed accurately and dissolved with 100 mL of methanol under ultrasound. The suspension was filtrated with a 0.22 μm syringe filter and 1 mL of the filtration was eluted with pure water to 20 mL. In the case of rutin capsules, they were hulled to obtain the average loading amount; The filtration was eluted with pure water to 250 mL; Other steps were consistent with tablets. In the case of *Flos Sophorae*, the pretreatment was referred to Chinese Pharmacopoeia (Edition 2020). *Flos Sophorae* was dried and smashed with a micromill respectively, and then 200 mg of the cribble was dissolved in methanol under ultrasound for 30 min. After cooling to room temperature, the suspension was filled volume to 50 mL with methanol and then filtrated. 1 mL of the filtration was diluted with pure water to 25 mL.

For real sample detection, 0.5 mL of CDs solution (100 μg mL^{-1}) was added to 4.0 mL of the foregoing sample solution. The mixture was incubated for 3 min at 25 °C and then the fluorescence intensity was determined at E_x of 355 nm and E_m of 430 nm. The quenching efficiency was obtained and put into the linear correlation equation to calculate the rutin concentration in each sample.

In the spiked recovery experiments, the sieved samples of rutin tablet, rutin capsules and *Flos Sophorae* (from PA1) were first spiked with rutin at three levels of 2.5, 15 and 25 μM and then treated according to the aforementioned procedure. The spiked recovery was calculated and evaluated.

For further assessment the accuracy of the proposed method, the contents of rutin in all the above samples were determined through HPLC method. The chromatographic conditions were as follows: an ODS column (4.6*250 mm, 5 μm, Shimadzu), methanol-1 % HAc (v/v: 32/68) as the mobile phase with a flow rate of 1.0 mL/min, detector wavelength set as 257 nm and injection volume of 10 μL. The standard curve was first obtained through the peak area and the corresponding concentration of rutin working solution series and then the real samples were injected to acquire the rutin content.

3. Results and discussion

3.1. Synthesis of CDs

Hydrothermal process is a popular and efficient method of preparing CDs owing to the cost-effectiveness, ease of operation, and simple equipment requirements. Nevertheless, QY of the CDs prepared with the cumin seeds bought from the market showed poor reproducibility in the pre-experiments. After verification and argumentation, heterogeneity of raw material should take the blame. Cumin seeds obtained from the market were usually a mixture of the whole grain (seed), shell (testa) and kernel (embryo) on account of the traditional harvest process. As far as we know, general plants embryos are rich in nutritional ingredients which are very different with testas mainly consisting of cellulose. Hence, sampling process could not be uniform in view of reality, thus resulting in poor reproducibility of QY. At the same time, we were also excited to attempt the separation of the raw material into two relatively uniform parts, i.e. testas and embryos, as Section 2.3 described. CDs derived from the whole seeds, testas and embryos were named CDs-S, CDs-T and CDs-E, respectively. When the same reaction conditions were applied, the QY of CDs-S, CDs-T and CDs-E were 7.46 %, 5.87 %, and 9.10 %, respectively with all the RSD below 5 % (n = 3). The discrepancy of QY may be attributed to the different composition of the testas and embryos. The main chemical component of testas is cellulose, which is a polysaccharide substance composed of C, H and O elements. While the embryos usually store a lot of fat, volatile oil, protein and other nutrients. It has been reported that the protein contents of cumin seeds from different origins are as high as 20 % (Merah et al., 2020). Thus CDs-E would theoretically inherit more N element from the cumin embryo, whereupon obtaining the highest QY, and the conclusion will be verified through characterization in the following part.

In addition, reaction conditions for preparing CDs-E including the hydrothermal reaction temperature, duration time and the input amount of cumin embryos were optimized individually. According to results displayed in Fig. 1, the optimal preparation conditions are 2.0 g powder dispersed in 10 mL ultrapure water and heated at 200 °C for 12 h. Under these conditions, QY can reach 10.60 %, which is higher than CDs prepared with other spices (Kaur et al., 2021).

3.2. Characterization of the CDs

A series of characterization were carried out to compare the differences between CDs prepared with different carbon source. As shown in Fig. 2(a ~ c), the three CDs were all homogeneously distributed on the matrix and spherical in shape. After counting and statistical analysis, they were all mainly distributed between 1.0 ~ 4.5 nm. The average particle size of CDs-T, CDs-S and CDs-E were 2.61 nm, 2.54 nm and 2.40 nm, respectively. CDs-E demonstrated a relatively smaller particle size than the other two, meaning greater quantum confinement, which may be responsible for the higher QY (Zhu et al., 2015, Ai et al., 2021, He et al., 2022). According to high-resolution TEM images, lattice fringes with an average spacing of 0.21 nm were all found in three CDs, which match the (1 0 0) crystal plane of graphite (Hu et al., 2015). Fig. 2d displayed the AFM images of CDs-E, which further demonstrated the size distribution of 1 ~ 5 nm. The three representative CDs captured in the image possessed the height of 2 ~ 3 nm. The graphite-like structure of CDs was further confirmed by the XRD pattern, which demonstrated a wide diffraction peak at 28.6° and a relatively weak peak at 43.0° (Fig. 2e) originating from the (0 0 2) and (1 0 0) lattice of graphite carbon, respectively (Gong et al., 2016).

The elemental composition and surface functional groups of CDs were characterized by XPS and FT-IR jointly. As shown in Fig. 3a, three common peaks at around 286 eV (C1s), 399 eV (N1s), and 532 eV (O1s) were observed in the XPS survey spectra of the three CDs, demonstrating that they are primarily composed of carbon, nitrogen and oxygen. Particularly, a weak peak at 133 eV attributed to the signal of P2p was observed in CDs-E (Yang et al., 2018), while invisible in the other two. The proportion of each element was calculated and displayed in Table 1. The proportions of carbon in the three CDs were close, and there were obvious differences in the composition of nitrogen and phosphorus. CDs-E possessed the highest proportion of nitrogen which may be attributed to the higher content of proteins in embryos. The trace phosphorus element is speculated to come from the phospholipids in cumin embryos, which are scarce in testas. In particular, it should be noted that the loss of P2p signal in CDs-S should be attributed to the dilution effect of testas, thus resulting in lower response which are difficult to be discerned by XPS. Each element was further analyzed by high-resolution XPS. As illustrated in Fig. 3, the high-resolution C1s XPS spectra of CDs were differentiated into three peaks locating at around 288 eV, 286 eV and 284 eV, which were assigned to C═O, C—O/C—N and C═C/C—C, respectively (Lv et al., 2020). The high resolution O1s spectrum showed two peaks at around 532 eV and 531 eV, confirming the existence of oxygen in the forms of C—O and C═O. In the high resolution N1s spectrum, the characteristic peaks at 399 eV and 400 eV were related to

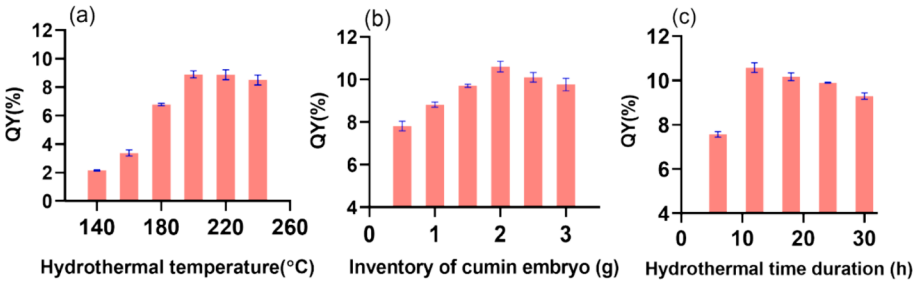

Fig. 1. Optimization of the preparation conditions for CDs-E with the quantum yield (QY%) as the indicator (n = 3). (a) Hydrothermal reaction temperature: (b) Input amount of cumin embryos. (c) Hydrothermal time duration.

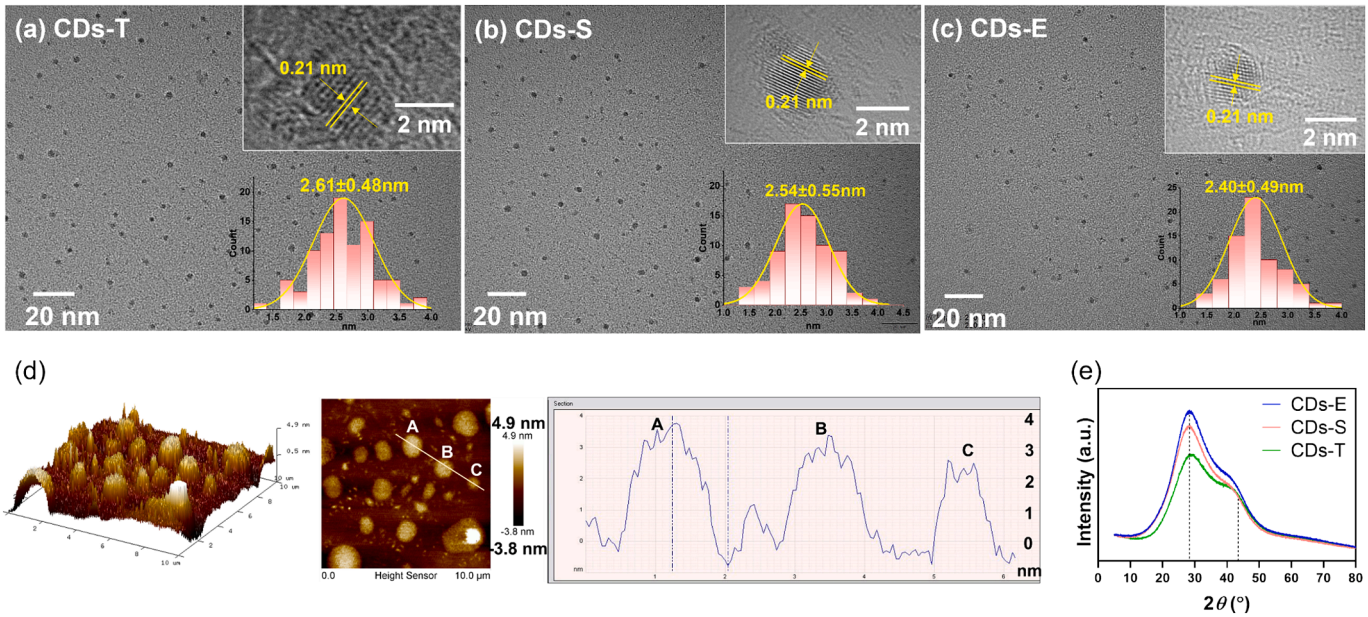

Fig. 2. Characterization of the morphology of three CDs. (a ~ c) TEM images (inset at top right: HRTEM image of single CD; inset at bottom right: size distribution); (d) AFM images for CDs-E; (e) XRD spectra.

the N—C, and N—H, respectively (Ma et al., 2020). Nitrogen doping can improve the fluorescence QY of CDs through two respects (Chen et al., 2019, Liu et al., 2019, He et al., 2022). On one hand, the N atom has 5 valence electrons, and the size is similar to the carbon atom. When N is embedded in the carbon structure to form the N-C bonds, the initial band gaps are regulated and new energy levels will form, producing new surface states (the so-called N-states). It can capture electrons and promote radiative recombination, eliminate or inhibit the original O-states and suppress non-radiative recombination, which can directly improve QY. On the other hand, the formation of amino group (—NH_2), which act as an electron donor, can promote π-electron conjugation in CDs, thus increasing the probability of electron transition from the ground state to the lowest excited single state, thereby indirectly increasing QY. Comparing the N1s spectra of the three CDs (Fig. 3(b3, c3, d3)), it can be observed that CDs-E had relatively more N—C and less N—H groups. While CDs-E possessed the highest QY, which implied that N-C may contributes more to the improvement of QY than N—H based on the above analysis. In the high-resolution P2p spectrum of CDs-E (Fig. 3 (c4)), two peak pairs at 133.0/133.8 eV and 133.5/134.9 eV were assigned to P-C/P = O and P-O respectively (Yang et al., 2018). Due to the trace level of phosphorus and the unclear mechanism, the effect of phosphorus on the QY of CDs-E is not discussed herein.

The FT-IR spectra of CDs were shown in Fig. 3e, some same absorption peaks at 3200 cm^{-1}, 2950 cm^{-1}, and 1760 cm^{-1} were observed which were related to the stretching vibration of O—H/N—H, C—H and C═C, respectively. The intensity of absorption peak at 1680 cm^{-1} was significantly higher for CD-E than for the other two CDs, indicating the presence of more C═O on the surface of CDs-E. Similarly, the intensity of absorption peaks at 1401 cm^{-1} and 1295 cm^{-1} of CDs-E were slightly higher which were attributed to C-N and C-O respectively (Li et al., 2018, Wang et al., 2023).

To sum up, The FT-IR and XPS analysis corroborated each other and confirmed the existence of hydrophilic groups jointly, such as –OH, –COOH, and –NH_2 on the surface of the prepared CDs, ensuring favorable water solubility and feasible modifiability. The CDs prepared with different parts of cumin seeds differed in QY, size, elemental and functional group composition. Embryos as carbon source could produce higher QY resulting from the smaller size and more content of N-doping. Consequently, a fine separation of raw materials can significantly improve the fluorescence performance of CDs derived from biomass.

3.3. *Optical properties and fluorescence stability of CDs-E*

The UV–vis absorption and fluorescence spectra were recorded to further investigate the optical properties. As shown in Fig. 4a, the solution of CDs-E exhibited a yellowish color in the daylight, and emitted blue fluorescence under UV light at 365 nm (inset). The UV–vis spectrum (orange line) of CDs-E showed a broad absorption in the range of 200 ~ 400 nm with two characteristic peaks at around 274 nm and 325 nm, which were severally assigned to the π–π* transition of C═C and the

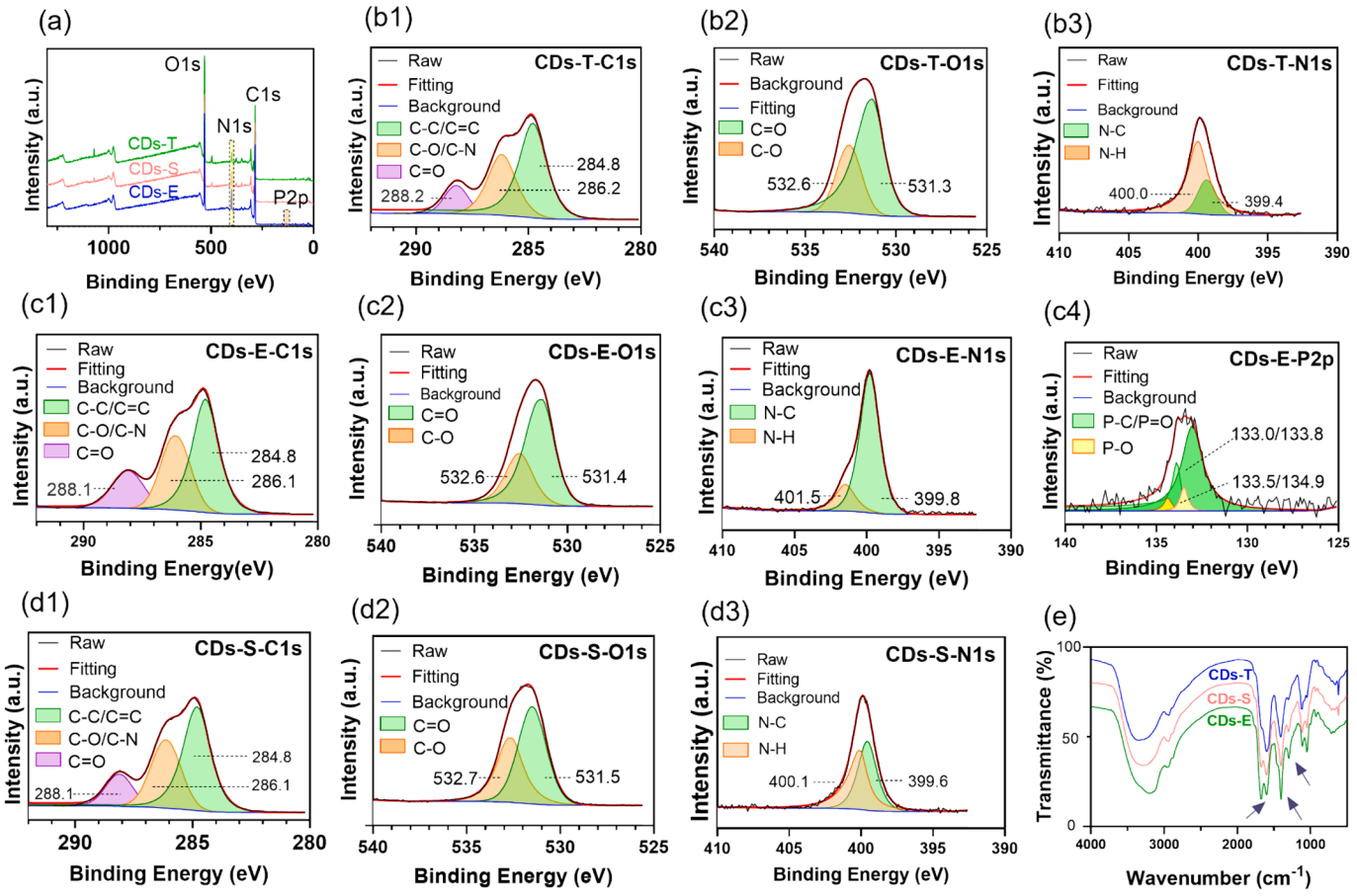

Fig. 3. Characterization of the elements and functional groups of three CDs. (a) Full scan XPS spectra; (b ~ d) High resolution XPS spectra of C1s, O1s, N1s and P2p; (e) FTIR spectra.

Table 1
The elemental composition of CDs calculated through XPS.

Element	CDs-T	CDs-S	CDs-E
C (%)	64.07	65.45	62.72
O (%)	31.28	27.42	27.46
N (%)	4.65	7.13	9.21
P (%)	–	–	0.61

n-π* transition of C═O. Both the excitation (pink line) and emission (green line) spectra of CDs-E covered a wide wavelength range. A maximum excitation wavelength of 355 nm and a maximum emission wavelength of 430 nm were observed. In addition, as the excitation wavelength increased, the fluorescence spectrum showed substantial redshift and fluorescence intensity changed constantly (Fig. 4b). The phenomenon of excitation-dependent emission can be explained by the varied surface functional groups and heterogeneity of particle size (Roy et al., 2015, Ai et al., 2021).

The fluorescence stability is one of the key characteristics of CDs which determines their potential in sensing applications. As shown in Fig. 5a, the fluorescence of CDs-E remained steady and relatively high at pH 3 ~ 10 and would decrease to a certain extent when pH was further reduced or increased. A possible explanation for this phenomenon is that the protonation and deprotonation states of the functional groups on the surface of CDs-E change greatly when the environment is too acidic or alkaline. As illustrated in Fig. 5b and 5c, even in the presence of high concentration of NaCl (1 mol/L) or prolonged exposure to ultraviolet light (120 min), the fluorescence of CDs-E only showed slight changes.

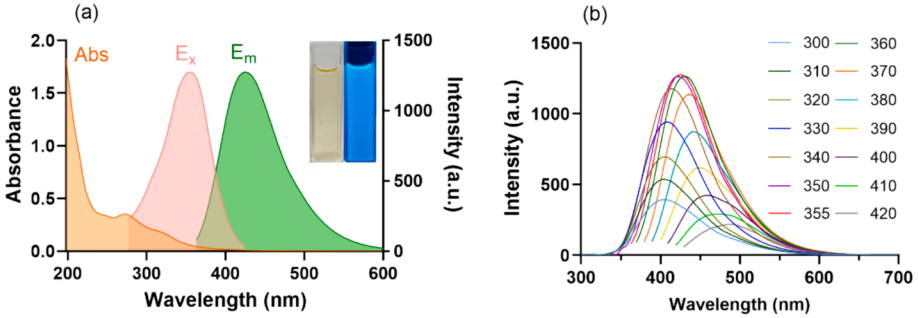

Fig. 4. Optical properties of CDs-E. (a) UV–vis absorption, fluorescent excitation (E_m = 430 nm) and emission (E_x = 355 nm) spectra of CDs-E (inset: photographs of CDs-E under daylight and UV lamp of 365 nm); (b) Fluorescent emission spectra of CDs-E under different excitation wavelengths from 300 to 420 nm.

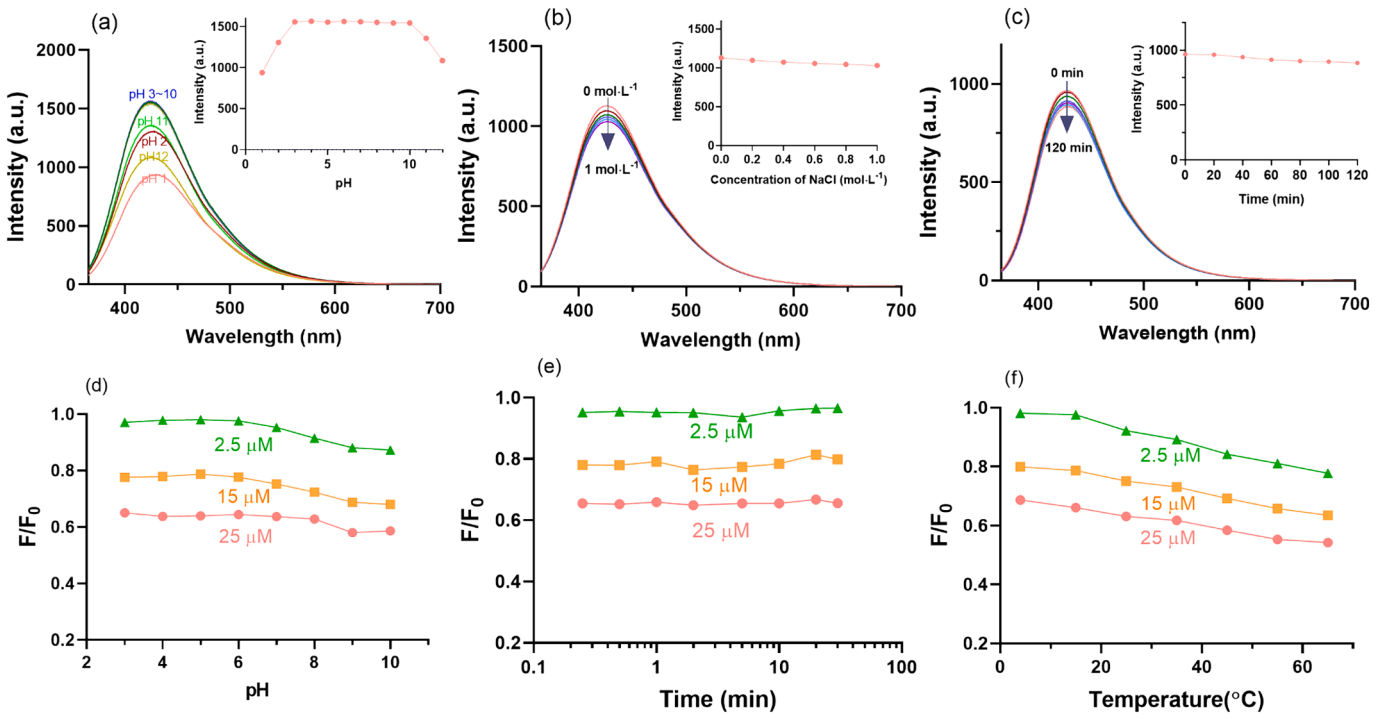

Fig. 5. Investigation of the stability of CDs-E (fluorescence emission spectra (E_x = 355 nm) of at (a) different pH, (b) ionic strength and (c) exposure time to ultraviolet light, inset; the responding fluorescence intensity under each condition at E_x = 355 nm and E_m = 430 nm) and optimization of the sensing conditions ((d) pH, (e) equilibrium time and (f) incubation temperature) for rutin at three concentration levels based on the CDs-E with quenching efficiency (F/F_0) as the indicator.

According to the above results, CDs-E was both salt-resistant and photostable, also had tolerance to normal pH environment, thus paving the way for the subsequent application in the detection of rutin.

3.4. *Fluorescence sensing of rutin*

It was found that the fluorescence of CDs could be quenched by rutin

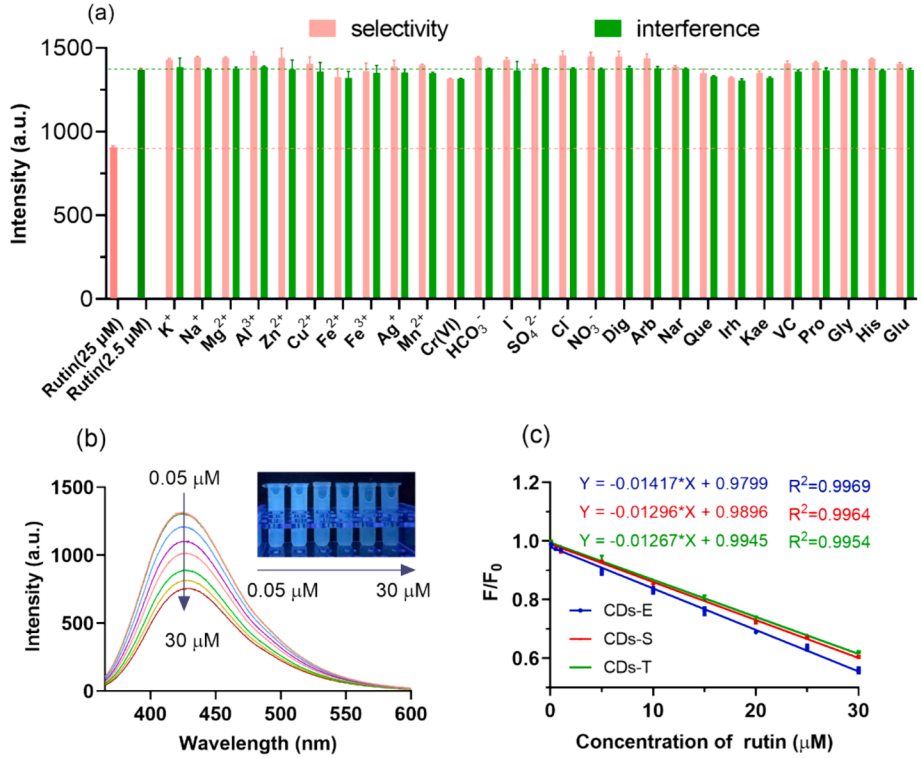

Fig. 6. Performance of the proposed rutin sensor. (a) Selectivity and anti-coexistence interference of sensor based on CDs-E; (b) The fluorescent emission spectra of CDs-E in the presence of rutin at different concentration (E_x = 355 nm) (inset: representative photographs of the mixture under UV light of 365 nm); (c) Linear fitting curves of quenching efficiency versus concentration of rutin based on the three CDs.

in pre-experiment, so the fluorescence sensors based on the three CDs for rutin detection were proposed and compared. To achieve the maximum sensitivity of CDs to rutin, the pH of the sensing system, equilibrium time and incubation temperature were optimized with CDs-E as an example and the results were displayed in Fig. 5(d ~ f). To obtain more convincing results, rutin solutions at different concentration levels (2.5 μM, 15 μM and 25 μM) were adopted. Given the fluorescence stability of CDs-E, pH optimization was only carried out within the range of 3 ~ 10. The results indicated that pH has almost no effect on the fluorescence quenching of CDs-E induced by rutin (Fig. 5d). After the addition of rutin into the CDs-E solution, the fluorescence intensity of CDs-E decreased instantly and remain stable (Fig. 5e). With the rise of incubation temperature, the quenching efficiency increased accordingly (Fig. 5f). This phenomenon was be relevant to the quenching mechanism, which will be discussed in later sections. Considering the feasibility and convenience of practical application, no pH adjustment, an equilibrium time of 3 min and incubation temperature of 25 °C were applied in the subsequent detection experiments.

As shown in Fig. 6a, the selectivity and anti-interference ability of the sensing system was satisfactory. When other chemicals added to the CDs-E solution instead of rutin at relatively high concentration (25 μM), including various inorganic salt ions, small organic molecule and herbal medicinal ingredients, the fluorescence intensity (pink bar) stayed nearly the same as F_0, which is far from the quenching efficiency of rutin at the same concentration level, indicating that the CDs-E sensing system was highly selective for rutin. Additionally, when these components added to the system with rutin simultaneously (interfering substance: 10 μM; rutin: 2.5 μM), the fluorescence response of the CDs-E to rutin in the mixed system (pink bar) showed no significant changes compared with control. The slight impacts of Fe^{2+} and Cr(VI) on the quenching process might be due to the redox reaction between them and the functional groups on CDs-E, while for Que, Irh and Kae, the similar structure with rutin should be the culprit. Considering the relatively high concentration of these substances (four times higher than rutin) applied in the experiments, the influence of them in reality could be ignored, which signifying the superior anti-interference ability of the sensor. The favorable selectivity of CDs towards rutin is speculated mainly due to the hydrogen bonding between the hydroxyl groups of rutin and the amine, amide and carboxyl groups of CDs. Also, the π-π interactions between the aromatic stack of CDs and rutin may facilitate the recognition process (Sinduja and John, 2018).

The fluorescence response of the sensors based on the three CDs to rutin was studied and compared quantitatively. According to Fig. 6b, the fluorescence intensity of CDs-E decreased gradually with an increase in rutin concentration from 0.05 to 30 μM. It can also be observed that the fluorescence of the solution decreases significantly under ultraviolet light as the concentration of rutin increases, which implies that the sensor has the potential for semi-quantitative visual detection of rutin. Correspondingly, favorable linear correlations were obtained between the quenching efficiency and the concentration of rutin as shown in Fig. 6c. The linear ranges of the sensors based on three CDs are relatively consistent. The LOD of CDs-E, CDs-S and CDs-T were calculated to be 0.015 μM, 0.016 μM and 0.017 μM respectively, according to 3σ/k, where σ is the standard deviation of the blank sample and k is the slope of the linear calibration curve. From the perspective of detection performance, there is no obvious difference, which may be due to the fact that their biomass sources are different parts of the same species. However, due to the high QY, CDs-E has higher fluorescence intensity under the same concentration and excitation conditions, which can reduce the detection error of the fluorescence spectrophotometer. Therefore, CDs-E was selected to construct the fluorescence sensor of rutin in the subsequent experiments. In comparison with other reported rutin sensing systems (Table 2), the proposed CDs-E sensor herein had comparable or better linear range and sensitivity. Based on these results, the sensor provided an optimal strategy for detection of rutin.

Table 2
The comparison of CDs-E and other reported CDs for sensing of rutin.

CDs Source	Quantum Yield (%)	Linearity Range (μM)*	LOD (μM)*	Ref
$[OMIM]BF_4$	14.87	1.0 ~ 100.0	0.06	Wang et al., 2023
citric acid + thiourea	24.1	0.16 ~ 655.7	0.05	Huang et al., 2022
molasses + thioacetamide + glycine	38.7	0.02 ~ 92.3	0.008	Mahmoud et al., 2022
citric acid + o-phenylenediamine	40.15	4.1 ~ 65.6	3.7	Xie et al., 2022
MES on MWCNTs	42.8	0.1 ~ 213.1	0.03	Li et al., 2019
$Na_2[Cu(EDTA)]$ + $NH_2OH{\cdot}HCl$	9.8	0.16 ~ 24.6	0.08	Wang et al., 2019
asparagine	–	0.50 ~ 15.0	0.10	Sinduja and John, 2018
cumin embryo	10.60	0.05 ~ 30.0	0.015	this work

* All the units have been converted into μM for ease of comparison with other reports.

3.5. Practical application in real samples

The rutin content in real samples including TCM (*Flos Sophorae* from different PA), chemical pharmaceutical (rutin tablets) and health care product (rutin capsules) were determined by the sensor based on CDs-E and the results were compared with which obtained through traditional HPLC method. As shown in Table 3, the measured content of rutin in these samples by the two methods were similar, confirming the reliability and accuracy of the sensing system. The measured content of rutin in tablets were nearly the same with their labeled content, which indicated that the drug is qualified. While, the content of the rutin in capsules (a health care product of certain brand) exceeded the label severely in both methods, which served as a warning for people with daily health care needs. The content of rutin in *Flos Sophorae* from different PA had significant differences, which conformed the reality. According to the quality control requirement in Chinese Pharmacopoeia, all the contents of rutin in the four batches meet the criterion (w% > 6 %).

Furthermore, three concentration levels of rutin were spiked into rutin tablets, rutin capsules and *Flos Sophorae* (from PA1) respectively and the spiked samples were analyzed through the proposed sensor. As shown in Table 4, the spiked recoveries were in the range of 82.46 % ~ 117.52 % and all the RSD were below 6.52 %, demonstrating the high precise and stability of this method. In summary, the sensor can be applied in quantitative determination of rutin in complex samples, showing the potential for practical applications not only in quality control of rutin-related drugs and health care products, but also authenticity identification and origin differentiation of TCM with rutin as the quality index.

3.6. Fluorescence quenching mechanism

A detailed investigation was conducted into the exploration of quenching mechanism of CDs-E by rutin as pioneering literature reviewed (Zu et al., 2017). Firstly, the interaction between rutin and the CDs-E was characterized by UV–vis spectroscopy. As shown in Fig. 7a, there were two wide absorption peaks at 255 nm and 352 nm of the UV–vis absorption spectrum for rutin (blue line). After the addition of CDs-E, the UV–vis absorption was significantly increased. While, this spectrum of the mixed solution (purple solid line) almost overlapped the graph merged with the spectrum of rutin and CDs-E (purple dotted line), excluding the possibility of static quenching since no new chemical bonds had been formed between rutin and CDs. Meanwhile, the excitation spectrum of the CDs-E was sufficiently covered by the UV absorption band of rutin at 280 ~ 400 nm, and a partial overlap was also

Table 3
Determination of rutin in practical samples through the proposed sensor based on CDs-E and HPLC method.

Sample			Labeled Content	Determined Content		
				This work		HPLC method
				AVG	RSD (%)	
Rutin Tablets			20 mg	20.20 mg	1.01	20.72 mg
Rutin Capsules			250 mg	359.52 mg	0.54	358.02 mg
Flos Sophorae	Producing area	1	w%>6%	6.75 %	2.13	6.86 %
		2		8.89 %	4.89	8.67 %
		3		9.73 %	2.49	9.72 %
		4		6.12 %	1.38	6.25 %

Table 4
Spiked recoveries of rutin determined through the constructed sensor based on CDs-E in practical samples at different spiked concentration levels.

Sample	Spiked Concentration (μM)	Recovery (n = 3	
		AVG (%)	RSD%
Rutin Tablets	2.5	82.46	4.23
	15	96.82	4.64
	25	97.90	1.70
Rutin Capsules	2.5	112.67	1.95
	15	117.52	1.26
	25	99.26	1.81
Flos Sophorae (PA1)	2.5	96.38	2.56
	15	93.47	2.70
	25	93.43	6.52

observed for the emission spectrum at the wavelength range of 360 ~ 400 nm. This phenomenon indicated the possible mechanism of inner filter effect (IFE) and fluorescence resonance energy transfer (FRET).

Secondly, as shown in Fig. 5f, the fluorescence quenching efficiency of CDs-E by rutin were accelerated with the increase of incubation temperature. It is conjectured that dynamic quenching mechanism may exist. To further verify the results, sensing assays with rutin solution series at different temperature were proceeded and the relationship between the rutin concentration (Q) and the F_0/F value at different temperature was plotted in Fig. 7b. Favorable linearities were observed and the Stern-Volmer constant (Ksv) was calculated through the equation $F_0/F = 1 + Ksv[Q]$, respectively. The results demonstrated that Ksv increases with the rise of temperature, which seems to be consistent with dynamic quenching mechanism.

Nevertheless, fluorescent decay curves of CDs-E in the absence and presence of rutin were examined (as displayed in Fig. 7c). The fluorescence lifetime of CDs-E showed negligible change before and after the addition of rutin CDs-E (5.08 ns and 4.81 ns respectively), thus ultimately excluding FRET and dynamic quenching.

Eventually, combining the phenomenon of no formation of new chemical bonds and the overlap between the absorbance spectrum of rutin and the fluorescence spectra of CDs-E, IFE became the only possible mechanism for explaining the quenching of CDs-E by rutin, which coincided with most reports (Wang et al., 2019, Mahmoud et al., 2022, Wang et al., 2023).

4. Conclusion

In this work, CDs derived from cumin embryos, testas and the whole seeds were prepared through hydrothermal method respectively and compared in detail. It was found that the fluorescence quantum yield of CDs-E was supreme, which may probably due to the smaller particle size and larger amount of C-N functional groups. Rutin could significantly quench the fluorescence of CDs-E through IFE, thus a highly efficient and selective fluorescence sensor for rutin detection was established and successfully applied in drugs, health care products and traditional Chinese medicines containing rutin. It is also anticipated that a fine separation of raw materials opens up a new avenue for the improvement of the QY of CDs based on biomass.

CRediT authorship contribution statement

Xiao-Lin Xie: Writing – original draft, Methodology, Conceptualization. **Zhao Zhang:** Methodology, Data curation, Conceptualization. **Wen Xiong:** Methodology. **Jie Wang:** Software. **Wei Gong:** Validation. **Wen Xu:** Methodology. **Shuang Cai:** Writing – review & editing, Project administration, Funding acquisition. **Jing Li:** Writing – review & editing, Supervision, Funding acquisition, Data curation, Conceptualization.

Declaration of competing interest

The authors declare that they have no known competing financial interests or personal relationships that could have appeared to influence

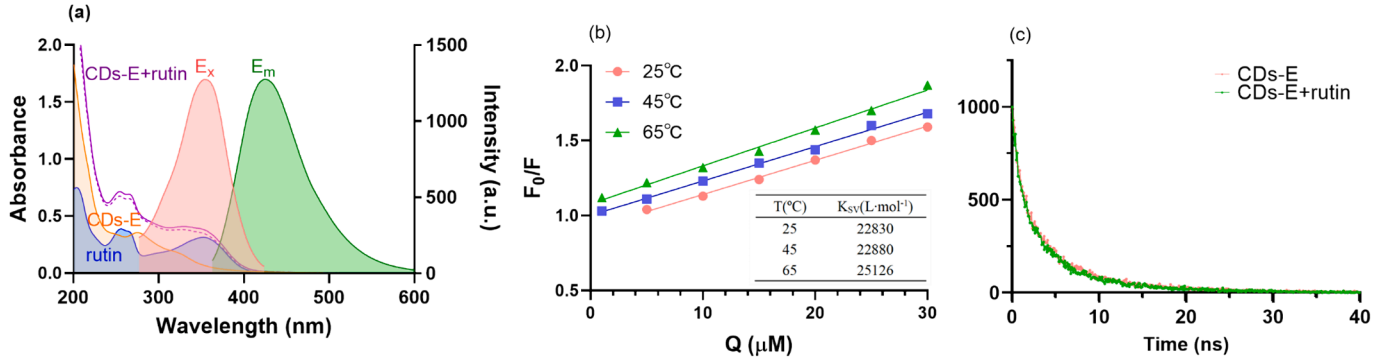

Fig. 7. Exploration of quenching mechanism of CDs-E by rutin. (a) UV–vis absorption spectra of rutin and CDs-E in the presence and absence of rutin, fluorescent excitation (E_m = 430 nm) and emission (E_x = 355 nm) spectra of CDs-E; (b) Stern-Volmer plots of the quenching of CDs-E by rutin at different temperature (ordinate: reciprocal value of quenching efficiency; abscissa: concentration of rutin) (inset: calculated Stern-Volmer quenching constant at different temperature); (c) Fluorescence lifetime decay curves of CDs-E in the presence and absence of rutin.

the work reported in this paper.

Acknowledgements

The authors gratefully acknowledge the financial support of Natural Science Foundation of Hubei Province (No. 2022CFB964) and the National Natural Science Foundation of China (No.32001009).

References

Ai, L., Yang, Y.S., Wang, B.Y., et al., 2021. Insights into photoluminescence mechanisms of carbon dots: advances and perspectives. Sci. Bull. 66, 839–856. https://doi.org/10.1016/j.scib.2020.12.015.

Chen, B.B., Liu, M.L., Li, C.M., et al., 2019. Fluorescent carbon dots functionalization. Adv. Colloid Interface Sci. 270, 165–190. https://doi.org/10.1016/j.cis.2019.06.008.

Chua, L.S., 2013. A review on plant-based rutin extraction methods and its pharmacological activities. J. Ethnopharmacol. 150, 805–817. https://doi.org/10.1016/j.jep.2013.10.036.

Gong, Y., Yu, B., Yang, W., et al., 2016. Phosphorus, and nitrogen co-doped carbon dots as a fluorescent probe for real-time measurement of reactive oxygen and nitrogen species inside macrophages. Biosens. Bioelectron. 79, 822–828. https://doi.org/10.1016/j.bios.2016.01.022.

Hasumura, M., Yasuhara, K., Tamura, T., et al., 2004. Evaluation of the toxicity of enzymatically decomposed rutin with 13-weeks dietary administration to Wistar rats. Food Chem. Toxicol. 42, 439–444. https://doi.org/10.1016/j.fct.2003.10.006.

He, C., Xu, P., Zhang, X.H., et al., 2022. The synthetic strategies, photoluminescence mechanisms and promising applications of carbon dots: current state and future perspective. Carbon 186, 91–127. https://doi.org/10.1016/j.carbon.2021.10.002.

Hu, Y., Yang, J., Jia, L., et al., 2015. Ethanol in aqueous hydrogen peroxide solution: hydrothermal synthesis of highly photoluminescent carbon dots as multifunctional nanosensors. Carbon 93, 999–1007. https://doi.org/10.1016/j.carbon.2015.06.018.

Huang, Y., Si, X.J., Han, M., et al., 2022. Rapid and sensitive detection of rutin in food based on nitrogen-doped carbon quantum dots as fluorescent probe. Molecules 27, 8834. https://doi.org/10.3390/molecules27248834.

Ji, C.Y., Zhou, Y.Q., Leblanc, R.M., et al., 2020. Recent developments of carbon dots in biosensing: a review. ACS Sensors 5, 2724–2741. https://doi.org/10.1021/acssensors.0c01556.

Kaur, A., Gupta, U., Hasan, I., et al., 2021. Synthesis of highly fluorescent carbon dots from spices for determination of sunset yellow in beverages. Microchem. J. 170, 106720 https://doi.org/10.1016/j.microc.2021.106720.

Li, L.-S., Jiao, X.-Y., Zhang, Y., et al., 2018. Green synthesis of fluorescent carbon dots from Hongcaitai for selective detection of hypochlorite and mercuric ions and cell imaging. Sens. Actuat. B-Chem. 263, 426–435. https://doi.org/10.1016/j.snb.2018.02.141.

Li, H., Xu, Y., Zhao, L., et al., 2019. Synthesis of tiny carbon dots with high quantum yield using multi-walled carbon nanotubes as support for selective “turn-off-on” detection of rutin and Al^{3+}. Carbon 143, 391–401. https://doi.org/10.1016/j.carbon.2018.11.049.

Liu, S., Cui, J., Huang, J., et al., 2019. Facile one-pot synthesis of highly fluorescent nitrogen-doped carbon dots by mild hydrothermal method and their applications in detection of Cr(VI) ions. Spectrochim. Acta. A. 206, 65–71. https://doi.org/10.1016/j.saa.2018.07.082.

Liu, S.H., Liu, Z.C., Li, Q.F., et al., 2021. Facile synthesis of carbon dots from wheat straw for colorimetric and fluorescent detection of fluoride and cellular imaging. Spectrochim. Acta. A. 246, 118964 https://doi.org/10.1016/j.saa.2020.118964.

Lv, X., Man, H., Dong, L., et al., 2020. Preparation of highly crystalline nitrogen-doped carbon dots and their application in sequential fluorescent detection of Fe^{3+} and ascorbic acid. Food Chem. 326, 126935 https://doi.org/10.1016/j.foodchem.2020.126935.

Ma, J., Zhang, H., Peng, F., et al., 2020. Carbon dots as fluorescent nanoprobe for the determination of N-acetyl-β-d-glucosaminidase activity. Anal. Chim. Acta. 1101, 129–134. https://doi.org/10.1016/j.aca.2019.12.018.

Mahmoud, A.M., Mahnashi, M.H., Al Fatease, A.M., et al., 2022. Fluorometric and electrochemical dual-mode detection of toxic flavonoid rutin based on new nitrogen and sulfur co-doped carbon dots: enhanced selectivity based on masking the interfering flavonoids with BSA complexation. J. Food Compos. Anal. 108, 104428 https://doi.org/10.1016/j.jfca.2022.104428.

Meng, W.X., Bai, X., Wang, B.Y., et al., 2019. Biomass-derived carbon dots and their applications. Energy Environ. Mater. 2, 172–192. https://doi.org/10.1002/eem2.12038.

Merah, O., Sayed-Ahmad, B., Talou, T., et al., 2020. Biochemical composition of cumin seeds, and biorefining study. Biomolecules 10, 1054. https://doi.org/10.3390/biom10071054.

Roy, P., Chen, P.-C., Periasamy, A.P., et al., 2015. Photoluminescent carbon nanodots: synthesis, physicochemical properties and analytical applications. Mater. Today. 18, 447–458. https://doi.org/10.1016/j.mattod.2015.04.005.

Sinduja, B., John, S.A., 2018. Sensitive determination of rutin by spectrofluorimetry using carbon dots synthesized from a non-essential amino acid. Spectrochim. Acta. A. 193, 486–491. https://doi.org/10.1016/j.saa.2017.12.067.

Wang, C.Y., Shang, S.Z., Zheng, X.D., et al., 2019. Fluorescent sensors based on Cu-doped carbon quantum dots for the detection of rutin. J. Brazil. Chem. Soc. 30, 988–996. https://doi.org/10.21577/0103-5053.20180245.

Wang, B.Y., Song, H.Q., Qu, X.L., et al., 2021. Carbon dots as a new class of nanomedicines: opportunities and challenges. Coordin. Chem. Rev. 442, 214010 https://doi.org/10.1016/j.ccr.2021.214010.

Wang, C.Z., Wang, X.J., Zhang, Y.P., et al., 2023. Ionic liquid-based carbon dots as highly biocompatible and sensitive fluorescent probe for the determination of vitamin P in fruit samples. Food Chem. 406, 134898 https://doi.org/10.1016/j.foodchem.2022.134898.

Wareing, T.C., Gentile, P., Phan, A.N., 2021. Biomass-based carbon dots: current development and future perspectives. ACS Nano 15, 15471–15501. https://doi.org/10.1021/acsnano.1c03886.

Xie, X.Q., Pan, M.F., Hong, L.P., et al., 2022. Carbon dots-embedded fluorescent molecularly imprinted photonic crystals hydrogel strip for accurate and selective detection of rutin in Sophora japonica products. Sensor. Actuat. B-Chem. 368, 132196 https://doi.org/10.1016/j.snb.2022.132196.

Yang, Y., Huo, D., Wu, H., et al., 2018. N, P-doped carbon quantum dots as a fluorescent sensing platform for carbendazim detection based on fluorescence resonance energy transfer. Sensor. Actuat. B-Chem. 274, 296–303. https://doi.org/10.1016/j.snb.2018.07.130.

Zhang, T., Ji, Q.X., Song, J.Y., et al., 2022. Preparation of nitrogen and sulfur co-doped fluorescent carbon dots from cellulose nanocrystals as a sensor for the detection of rutin. Molecules 27, 228021. https://doi.org/10.3390/molecules27228021.

Zhu, S.J., Song, Y.B., Zhao, X.H., et al., 2015. The photoluminescence mechanism in carbon dots (graphene quantum dots, carbon nanodots, and polymer dots): current state and future perspective. Nano Res. 8, 355–381. https://doi.org/10.1007/s12274-014-0644-3.

Zu, F.L., Yan, F.Y., Bai, Z.J., et al., 2017. The quenching of the fluorescence of carbon dots: a review on mechanisms and applications. Microchim. Acta. 184, 1899–1914. https://doi.org/10.1007/s00604-017-2318-9.